On Nonlinear Control of Single-Phase Converters With Active Power Decoupling Function

Huawei Yuan, *Student Member, IEEE*, Sinan Li, *Member, IEEE*, Wenlong Qi, *Student Member, IEEE*, Siew-Chong Tan, *Senior Member, IEEE*, and Shu-Yuen (Ron) Hui, *Fellow, IEEE*

***Abstract*—In this paper, a nonlinear controller is presented for regulating an emerging class of high power density, high power-conversion efficiency, and high reliability (H^3) single-phase power converters featuring small buffering capacitors. The proposed controller combines the best features of input–output feedback linearization and an automatic-power-decoupling (APD) control strategy, and achieves enhanced dynamic performances as compared to existing solutions based on linear control techniques. By feedback linearization, the plant models of H^3 single-phase converters are fully linearized and decoupled, and thus fast dynamics, large-signal asymptotic tracking, and global stability can be achieved with simple linear controllers. Additionally, the APD strategy further strengthens the robustness of the closed-loop system as active pulsating power buffering (of the instantaneous power difference between the ac-port and the dc-port of the converter) of basically any form can be achieved. With the proposed nonlinear controller, we are able to further exploit the potential and unlock several new features intrinsic in H^3 single-phase converters, e.g., active voltage holdup function, allowing extended holdup time (comparable to existing products with large dc-link capacitors) with only a small energy storage. The general theory, design procedures, and practical considerations of the nonlinear controller are detailed. A 100-W hardware prototype is also built to demonstrate the advantages of the proposed solution. New opportunities of H^3 single-phase power converters with the aid of the proposed nonlinear control are also suggested for future research.**

***Index Terms*—Automatic-power-decoupling (APD) control, feedback linearization, nonlinear control, single-phase converters.**

I. Introduction

SINGLE-PHASE power converters are widely used both in consumer and industrial electronics applications. Typical applications range from low-power applications (e.g., laptop adaptors, LED drivers, typically <250 W) up to kilowatt-scale medium-power applications (e.g., microinverters, electric vehicle chargers). Recently, there is a trend toward high power

Manuscript received January 15, 2018; revised May 14, 2018; accepted August 20, 2018. Date of publication September 2, 2018; date of current version April 20, 2019. This work was supported by the Hong Kong Research Grant Council under GRF Project 17205817. Recommended for publication by Associate Editor Dr. M. Ordonez (GE). *(Corresponding author: Sinan Li.)*

H. Yuan, S. Li, W. Qi, and S.-C. Tan are with the Department of Electrical and Electronic Engineering, The University of Hong Kong, Hong Kong (e-mail:

system's stability for constant-power-load operation during the steady state, may still lead to substantial system oscillations (e.g., with a dc-link voltage oscillation of $\pm 10\%$ of the average dc-link voltage) when the load power contains some random-frequency small-signal power variations. It appears that linear control techniques pose certain limitations for controlling H^3 single-phase converters. Some nonlinear control methods have been proposed recently and successfully implemented for regulating H^3 single-phase converters. In [10], a patent-pending feedforward controller is proposed aimed at large-signal operation. It achieves fast dynamics and strong robustness without voltage overshoot/undershoot in the dc-link in the event of a large step change of the load power. An alternative control method based on partial feedback linearization techniques is studied in [9], in which improved dynamic performance and robustness have been demonstrated in more experimental tests (e.g., grid voltage sag/swell, a step change of the dc-link voltage reference, etc.) for power-factor correction applications. Although experimental results have been positive in confirming that nonlinear controllers are more suitable for regulating the H^3 single-phase converters than linear ones, there is a lack of theory that can fully support the hypothesis. Moreover, reported controllers are topology dependent. There is no general control theory that can be applied to a wider range of H^3 single-phase converters.

2) *Holdup function:* Voltage holdup (often related to ac main failure) is mandatory in many ac-to-dc applications, such as PC adaptors and many consumer electronics products. Compared to their conventional counterpart, H^3 single-phase power converters featuring very small energy storage are generally believed to be incapable of providing voltage holdup function. This is probably one of the major hindrances in the industry for a wider application of H^3 single-phase power conversion technology.
3) *Ancillary services:* It is widely known that conventional single-phase power converters (e.g., full-bridge converters) are capable of providing several ancillary services, such as reactive power generation, bidirectional power flow control, and active power filtering (APF). Multifunctional single-phase power converters that can provide several ancillary services at the same time besides power conversion have been a hot topic in recent years [11]. These converters integrating multiple functions help improve overall system resiliency and reduce system cost drastically. To date, no attention has been given to employing the new-generation H^3 single-phase power converters to provide ancillary services. A highly compact and energy-efficient multifunctional single-phase power converter is highly desirable.

In this paper, the three challenges mentioned above are tackled in H^3 single-phase power converter design. It will be demonstrated how the three challenges can be solved simultaneously with a nonlinear control technique. In Section II, the key differences in the circuit operation between H^3 single-phase ac-to-dc converters and their conventional single-phase counterparts are analyzed. A theoretical framework is then established to explain the limitations of employing conventional linear controllers for regulating H^3 single-phase converters. In Section III, a nonlinear controller that is based on 1) input–output feedback linearization technique and 2) automatic power decoupling strategy, is presented. This controller allows the converter to operate with fast dynamics, global stability, and enhanced robustness at theoretically all operating conditions. In Section IV, the control method is applied to an H^3 single-phase power converter with a buck-type power-pulsation buffer that is operating in discontinuous conduction mode (DCM) to demonstrate its generality. The detailed design procedures and key considerations of the control are also explained. In Section V, a comprehensive performance evaluation of the simulations and experimental results is performed, showcasing the superiority of the control technique and suggesting new opportunities of H^3 single-phase power conversion technologies in future applications. In Section VI, the conclusion of this paper is drawn.

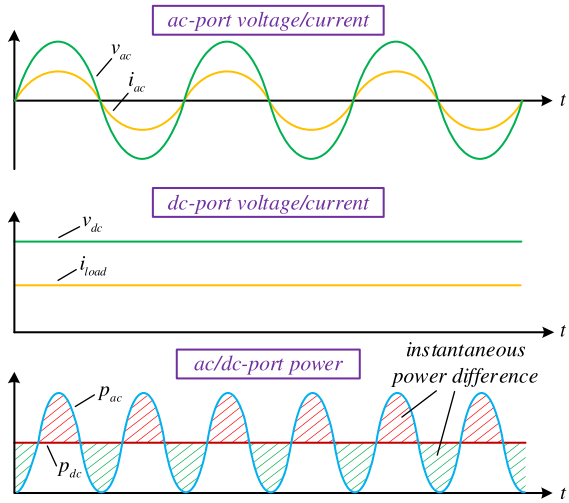

Fig. 1. DC- and ac-port operation waveforms of the H^3 single-phase converters in steady state.

II. Limitations of Applying Linear Controllers Over H^3 Single-Phase Converters

A. Characteristics of Conventional and New-Generation H^3 Single-Phase Power Converters

Single-phase ac-to-dc converters inherently require substantial energy storage in order to maintain a stable dc-link voltage [12], [13]. This energy-storage requirement cannot be reduced by increasing the switching frequency, as it depends on the instantaneous power difference between the ac-port and the dc-port of the system (see Fig. 1). Historically, the need for energy storage has been solved passively, e.g., by directly paralleling electrolytic capacitors (E-caps) on the dc-link [see $C_{\rm b}$ in Fig. 2(a)]. Such passive solution offers a good compromise between size and cost. However, E-caps have been widely known to be less reliable with limited service lifetime (e.g., <7000 h at 105 °C [14], [15]). Additionally, as C_b and the dc-port are electrically coupled, the capacitance of C_b must be huge to meet the stringent requirement of the dc-link voltage ripple. In the new generation of H^3 power converters, the energy-storage function

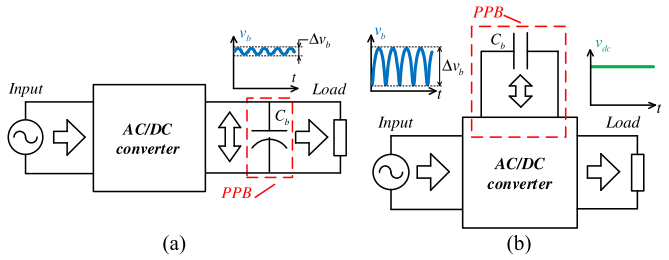

Fig. 2. Generic physical model of (a) conventional single-phase converters with a large dc-link capacitor and (b) H^3 single-phase converters with a small buffering capacitor at the ripple port [1].

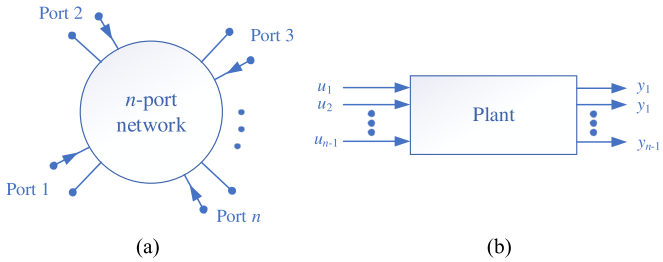

Fig. 3. (a) Physical n-port passive network and (b) its plant's model with multiple-input, multiple-output $(n \times n)$.

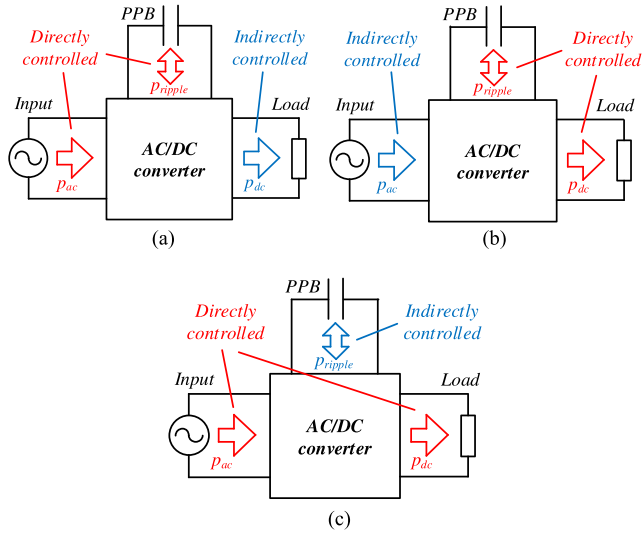

Fig. 4. Power flow diagram of the H^3 single-phase converters with the adoption of (a) *Strategy A*. (b) *Strategy B*. (c) *Strategy C*.

is achieved actively by diverting the imbalanced power into a ripple port [see Fig. 2(b)]. As C_b and the dc-port are electrically decoupled, the capacitance of C_b can be drastically reduced by allowing a much larger voltage fluctuation Δv_b over the ripple port while still maintaining a steady dc-link voltage. As a result, compact and reliable single-phase power converter design can be simultaneously achieved by replacing E-caps with ceramic (or film) capacitors. In literature, the electrical circuit for achieving active energy storage is referred to as power-pulsation buffer (PPB) [10]. Essentially, the conventional single-phase converter can be described as a two-port passive network (with an ac-port and a dc-port), while the converter with an active PPB is a three-port one (with an additional ripple port). Three key differences regarding their circuit operation are identified as follows.

1) Small-Signal Versus Large-Signal Operation: The voltage fluctuation Δv_b in Fig. 2(b) is generally much larger than that in Fig. 2(a). For instance, in typical photovoltaic (PV) inverter applications, Δv_b in Fig. 2(a) must be less than 8.5% of the average dc-link voltage $V_{\rm dc}$ to attain a high energy utilization ratio [16], while Δv_b as large as 100% of $V_{\rm dc}$ is theoretically feasible in Fig. 2(b) in order to minimize C_b [1]. Therefore, the H^3 single-phase converter inherently involves large-signal operation at the ripple port even in the steady state. Conventional linear control techniques, which are based on small-signal approximations and valid only around specific operating points, hence, may not retain satisfactory dynamic performance and robustness, even during the steady state.

2) Large Versus Small DC-Link Inertia: In Fig. 2(a), the dc-port can be regarded as a voltage source as a large C_b is connected to the dc-link. $v_{\rm dc}$ is, hence, almost immune to the disturbances from the load and the ac-port provided that the interval of the disturbances is short. In contrast, no large capacitor but just some small ones for high-frequency filtering [not shown in Fig. 2(b)] are connected to the dc-link in Fig. 2(b). The small "inertia" of the dc-port tends to destabilize the overall system and $v_{\rm dc}$ becomes highly susceptible to disturbances from the load, the ac-port, and the ripple port. Therefore, linear control techniques applied to conventional single-phase converters may be ineffective to suppress the substantially increased impacts of external disturbances on H^3 single-phase power converters.

3) Single-Input Single-Output Versus Two-Input Two-Output: For a physical n-port passive network, the power of at most $n-1$ ports can be directly and independently controlled, following the principle of conservation of energy. To complement the $n-1$ control outputs, at least $n-1$ control inputs are needed (one for each port). Therefore, a physical n-port passive network is essentially an $n-1$-input $n-1$-output system from the control viewpoint, as highlighted in Fig. 3. This means that the conventional single-phase converter, being a physical two-port network, has a single-input single-output (SISO) plant's model, while an H^3 single-phase converter, being a physical three-port network, has a two-input two-output (TITO) plant's model. One major challenge for controlling a multiple-input multiple-output system is that the system states and the control inputs are generally coupled. The intrinsic coupling characteristic of the H^3 single-phase converter that is seldom considered in prior arts is another reason behind the poor dynamic performance with a linear controller.

B. Control Strategies for H^3 Single-Phase Power Converters

In addition to circuit operation, the control strategies also have major impacts on the overall system performance [9], [17]. As the targeted system is a three-port passive network, only the power of two out of the three ports can be directly controlled. As a result, there are following three possible control strategies (see Fig. 4):

Strategy A: direct control of ac- and ripple-port power;
Strategy B: direct control of dc- and ripple-port power;
Strategy C: direct control of ac- and dc-port power.

Strategy A and *Strategy B* involve direct control of the ripple-port power and are, thus, referred to as direct-power -decoupling

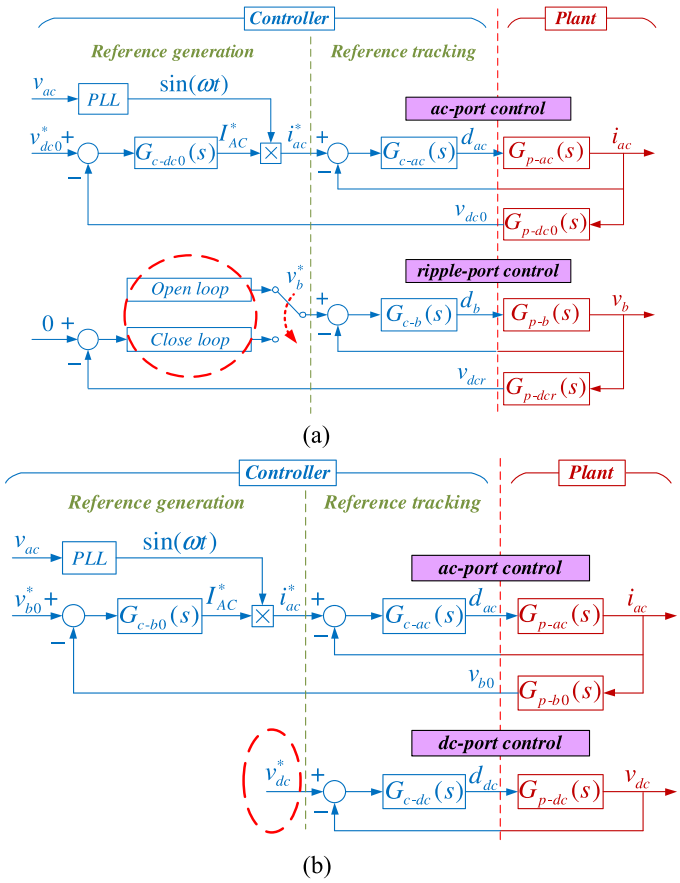

Fig. 5. Typical control structures of DPD control and APD control based on linear controllers.

(DPD) control. However, no dedicated ripple-port power control is required (indirect) with *Strategy C*. Such a control strategy is referred to as automatic-power-decoupling (APD) control [9]. In literature, *Strategy A* is widely adopted.

Although the three control strategies are theoretically equivalent and are expected to achieve the same dynamic performance, DPD control in practice is less robust and possibly leads to a more complicated control structure than APD control [9]. The reason can be explained using Fig. 5, which shows the typical control structures for DPD control (*Strategy A*) and APD control based on linear controllers.

As DPD control strategy involves direct ripple-port power regulation, a reference signal for the ripple port needs to be generated [e.g., v_b^* in Fig. 5(a)]. Essentially, the reference should be generated in such a way that the instantaneous power absorbed/released by the energy storage C_b match precisely the instantaneous power difference between the ac-port and the dc-port (i.e., $p_{\text{ripple}}(t) = p_{\text{ac}}(t) - p_{\text{dc}}(t)$, assuming the power losses of the converter are neglected). Two methods have been widely employed for ripple-port reference generation: 1) open-loop calculation based on the principle of conservation of energy [10], [13] and 2) forming an outer closed loop such that the dc-port has zero voltage ripples (i.e., $v_{\text{dcr}} \to 0$) [18]. The problem with these two methods is that they are more suitable for steady-state operation. In the event of a step change of the input voltage/load/reference, there will be a step change of $p_{\text{ac}}(t)$ and/or $p_{\text{dc}}(t)$, leading to a step change of $p_{\text{ripple}}(t)$ that needs to be buffered by C_b. Regarding the open-loop reference generation method, the exact amount of $p_{\text{ripple}}(t)$ is difficult to be calculated precisely and in real time, unless many sensors for measuring $p_{\text{ac}}(t)$ and $p_{\text{dc}}(t)$ are installed and a fast computational unit is used [10]. Regarding the closed-loop reference generation method, the control bandwidth in an outer loop is generally slow and insufficient for fast reference generation. It should be emphasized that any mismatch between the estimated and the true $p_{\text{ripple}}(t)$ will result in anomalies at the ac- or dc-port, leading to overshoot/undershoot in the system or even system instability. In contrast, no ripple-port reference generation is needed with the APD strategy as no dedicated ripple-port control is involved. Meanwhile, as the dc-port reference V_{dc}^* [see Fig. 5(b)] is usually a known quantity predetermined by specifications, dc-port regulation can be completed in a single control loop. If perfect reference tracking is achieved at the ac-port and the dc-port, the power imbalance $p_{\text{ripple}}(t)$ of basically any form shall be automatically transferred into the ripple port. That is, perfect pulsating power buffering can be achieved under theoretically all operating conditions. Therefore, APD control strategy is potentially more robust than DPD. The major problem with the reported APD control methods is that the controller is implemented with linear control techniques; thus perfect reference tracking is difficult [19]–[21].

The new characteristics of H^3 single-phase converters regarding the circuit operation and the limitations of previous control strategies suggest the following desired control concept: On the one hand, we want to model and deal with the nonlinearities and the couplings by using nonlinear control techniques, hopefully yielding more robust and superior dynamic performance; on the other hand, we want to employ APD control strategy to simplify the control structure and further enhance the system's robustness. Our proposed control method, which is to be explained below, represents a hybrid solution that combines the best features of these two approaches. As will be shown in the following sections, the proposed solution achieves very fast dynamics performance, strong robustness against external disturbances, and global stability with a very simple control structure.

III. General APD Control Method Based on Input–Output Feedback Linearization

Feedback linearization offers a powerful tool for controlling a multi-input multi-output (MIMO) nonlinear system [22]. It can completely solve the coupling and nonlinearity problem by algebraically transforming the input $\boldsymbol{u}$ of the original MIMO system such that the MIMO system becomes several fully linear and decoupled SISO subsystems with respect to the new control input $\boldsymbol{v}$. Importantly, simple linear control design techniques can then be applied to the SISO subsystems, yielding global stability of the original MIMO system. This simple concept of feedback linearization was first introduced in motor driver applications in [23], where many electrical and mechanical dynamics in the system were coupled. Later, it found wide applications in the areas of power electronics domain, such as solving various coupling issues (e.g., the d-q coupling) in the control of three-phase PWM converters [24].

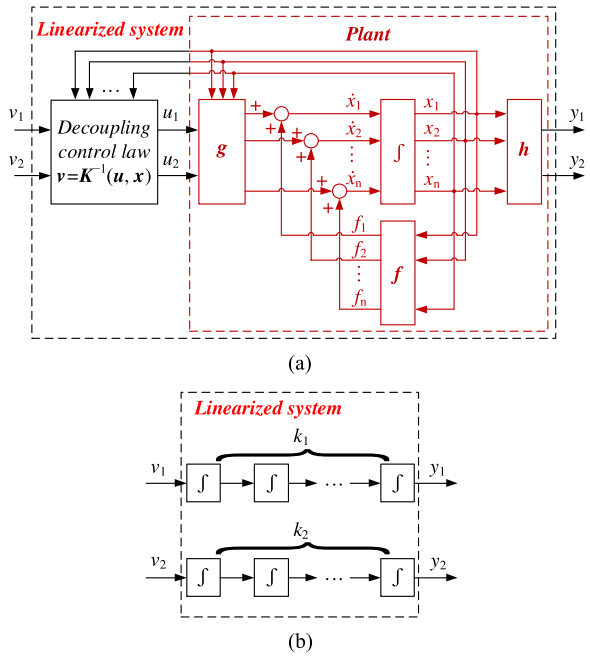

Fig. 6. (a) Block diagram of the nonlinear model of single-phase power converter with input–output feedback linearization. (b) Resultant equivalent block diagram after input–output feedback linearization.

Fig. 6 depicts the overall block diagram of the proposed nonlinear controller based on input–output feedback linearization and the APD control strategy, and the resultant equivalent block diagram after linearization. In particular, the H^3 single-phase converter, which is a TITO nonlinear system, is described in the following form:

$$\begin{cases} \dot{\boldsymbol{x}} = \boldsymbol{f}(\boldsymbol{x}) + \boldsymbol{g}(\boldsymbol{x}) \cdot \boldsymbol{u} \\ \boldsymbol{y} = \boldsymbol{h}(\boldsymbol{x}) \end{cases} \tag{1}$$

where $\boldsymbol{x} = [x_1, x_2 \ldots x_n]^{\mathrm{T}}$ is the state vector, n is the order of the TITO system, $\boldsymbol{f}$ and $\boldsymbol{h}$ are smooth vector fields, $\boldsymbol{g}$ is a smooth matrix, and $\boldsymbol{u} = [u_1, u_2]$ and $\boldsymbol{y} = [y_1, y_2]^{\mathrm{T}}$ are the two-dimensional input and output vectors. According to the APD control strategy, the ac- and the dc-port dynamics should be chosen as the control outputs y_1 and y_2, respectively.

To linearize the system, iteratively apply differentiation to each control output $y_i (i \in \{1, 2\})$ for k_i times until at least one control input $u_j (j \in \{1, 2\})$ appears in the expression of the derivative of y_i (i.e., the coefficient of u_j becomes nonzero), that is

$$y_i^{(k_i)} = L_f^{(k_i)} h_i(\boldsymbol{x}) + \sum_{j=1}^{2} L_{g_j} L_f^{(k_i - 1)} h_i(\boldsymbol{x}) \cdot u_j \tag{2}$$

where there exists at least one element $j \in \{1, 2\}$ such that

$$L_{g_j} L_f^{(k_i - 1)} h_i(\boldsymbol{x}) \neq 0 \tag{3}$$

where $L_f h$ and $L_g h$ are the Lie derivatives of $h(x)$ with regard to $f(x)$ and $g(x)$, respectively. Equation (2) can, thus, be rearranged in a compact matrix form as

$$\begin{bmatrix} y_1^{(k_1)} \\ y_2^{(k_2)} \end{bmatrix} = \boldsymbol{\alpha}(\boldsymbol{x}) + \boldsymbol{E}(\boldsymbol{x}) \cdot \boldsymbol{u} \tag{4}$$

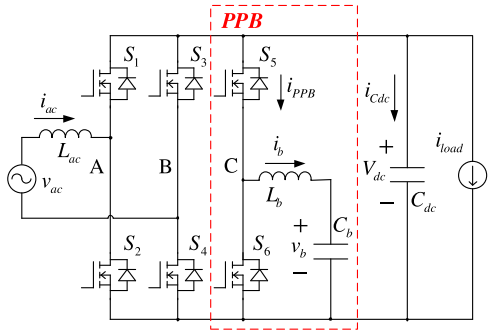

Fig. 7. Topology of the studied H^3 single-phase power converter with a buck-type PPB.

where

$$\boldsymbol{\alpha}(\boldsymbol{x}) = \begin{bmatrix} L_f^{(k_1)} h_1(\boldsymbol{x}) \\ L_f^{(k_2)} h_2(\boldsymbol{x}) \end{bmatrix}$$

$$\boldsymbol{E}(\boldsymbol{x}) = \begin{bmatrix} L_{g_1} L_f^{(k_1 - 1)} h_1(\boldsymbol{x}) & L_{g_2} L_f^{(k_1 - 1)} h_1(\boldsymbol{x}) \\ L_{g_1} L_f^{(k_2 - 1)} h_2(\boldsymbol{x}) & L_{g_2} L_f^{(k_2 - 1)} h_2(\boldsymbol{x}) \end{bmatrix}. \tag{5}$$

To linearize the original system (4), a new set of control inputs $\boldsymbol{v}$ can, thus, be selected as

$$\begin{bmatrix} y_1^{(k_1)} \\ y_2^{(k_2)} \end{bmatrix} = \begin{bmatrix} v_1 \\ v_2 \end{bmatrix} = \boldsymbol{v}. \tag{6}$$

By combining (4)–(6), $\boldsymbol{u}$ can be explicitly resolved from $\boldsymbol{v}$ according to the following control law:

$$\boldsymbol{u} = \boldsymbol{E}^{-1}(\boldsymbol{x}) \cdot (\boldsymbol{v} - \boldsymbol{\alpha}(\boldsymbol{x})) \tag{7}$$

provided that $\boldsymbol{E}(\boldsymbol{x})$ is nonsingular. By setting the output feedback law as

$$\begin{bmatrix} v_1 \\ v_2 \end{bmatrix} = \begin{bmatrix} y_1^{*(k_1)} + a_{1\,k_1-1} e_1^{(k_1-1)} + \cdots + a_{11} e_1^{(1)} + a_{10} e_1 \\ y_2^{*(k_2)} + a_{2\,k_2-1} e_2^{(k_2-1)} + \cdots + a_{21} e_2^{(1)} + a_{20} e_2 \end{bmatrix} \tag{8}$$

the closed-loop error dynamics of the system can be described by combining (6) and (8) as

$$\begin{cases} e_1^{(k_1)} + a_{1\,k_1-1} e_1^{(k_1-1)} + \cdots + a_{11} e_1^{(1)} + a_{10} e_1 = 0 \\ e_2^{(k_2)} + a_{2\,k_2-1} e_2^{(k_2-1)} + \cdots + a_{21} e_2^{(1)} + a_{20} e_2 = 0 \end{cases} \tag{9}$$

where $e_i = y_i^* - y_i$. It is, thus, easily to determine the coefficient of a_{ik} such that the error dynamics described in (9) are stable and can quickly converge to zero by regular linear control technique (e.g., pole-placement).

In [9], a partial feedback linearization-based controller without considering the nonlinearity introduced by the load current has been presented for a type of H^3 single-phase converters operating in the continuous conduction mode (CCM). To demonstrate the generality of this control method and to detail further design considerations that are missing in [9] (e.g., global stability analysis, and robustness against component variations), we focus on a type of H^3 single-phase power converters as shown in Fig. 7. The converter comprises a full-bridge converter ($S_1 - S_4, L_{\mathrm{ac}}, C_{\mathrm{dc}}$) and a buck-type active PPB

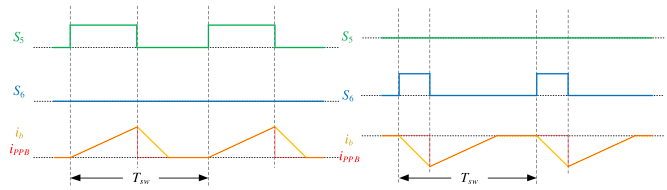

Fig. 8. Switching states of S_5 and S_6, and operating waveforms of i_b and i_{PPB} when the PPB operates in (a) the buck mode and (b) the boost mode.

(S_5, S_6, L_b, C_b). The buck-type PPB among all other alternatives is selected due to its highest achievable power density [10]. Different from the design in [10], the filter inductor L_b is deliberately designed to operate in DCM aiming to further improve the system's power density.

IV. Analysis of the Proposed Nonlinear APD Controller

A. Modeling of the H^3 Single-Phase Power Converter With a Buck-Type PPB

As the PPB must support bidirectional power flow to enable pulsating power buffering, the converter in Fig. 7 has two operation modes. Given the direction of the input current of the PPB, i_{PPB}, as marked in Fig. 7, the following observations are made.

1) When $i_{\mathrm{PPB}} > 0$ (the PPB absorbs power), the PPB operates in the buck mode. S_5 is actively switching at high frequency and S_6 remains OFF [see Fig. 8(a)].
2) When $i_{\mathrm{PPB}} < 0$ (the PPB releases power), the PPB operates in the boost mode. S_6 is switching at high frequency and S_5 remains OFF [see Fig. 8(b)].

The state-space-averaged model of the system over one switching period T_{sw} can be described by (1), which is restated as the following:

$$\dot{\boldsymbol{x}} = \boldsymbol{f}(\boldsymbol{x}) + \boldsymbol{g}(\boldsymbol{x}) \cdot \boldsymbol{u} \tag{10}$$

where

$$\boldsymbol{x} = \begin{bmatrix} x_1 \\ x_2 \\ x_3 \end{bmatrix} = \begin{bmatrix} i_{\mathrm{ac}} \\ v_{\mathrm{dc}} \\ v_b \end{bmatrix}, \boldsymbol{u} = \begin{bmatrix} u_1 \\ u_2 \end{bmatrix} = \begin{bmatrix} m \\ d_{\mathrm{PPB}}^2 \end{bmatrix}, \boldsymbol{f}(\boldsymbol{x}) = \begin{bmatrix} \frac{v_{\mathrm{ac}}}{L_{\mathrm{ac}}} \\ -\frac{i_{\mathrm{load}}}{C_{\mathrm{dc}}} \\ 0 \end{bmatrix}$$

$$\boldsymbol{g}(\boldsymbol{x}) = \begin{cases} \begin{bmatrix} -\frac{x_2}{L_{\mathrm{ac}}} & 0 \\ \frac{x_1}{C_{\mathrm{dc}}} & -\frac{(x_2 - x_3)}{cC_{\mathrm{dc}}} \\ 0 & \frac{x_2(x_2 - x_3)}{cC_b x_3} \end{bmatrix}, \text{ buck mode} \\ \begin{bmatrix} -\frac{x_2}{L_{\mathrm{ac}}} & 0 \\ \frac{x_1}{C_{\mathrm{dc}}} & \frac{x_3^2}{cC_{\mathrm{dc}}(x_2 - x_3)} \\ 0 & -\frac{x_2 x_3}{cC_b(x_2 - x_3)} \end{bmatrix}, \text{ boost mode} \end{cases} \tag{11}$$

m is the modulation index of the full-bridge converter, d_{PPB} is the duty cycle of the PPB (i.e., the duty cycle of S_5 during buck-mode operation and that of S_6 during boost-mode operation), and $c = 2L_b/T_{\mathrm{sw}}$.

For control convenience, the control output is selected as

$$\boldsymbol{y} = \begin{bmatrix} y_1 \\ y_2 \end{bmatrix} = \begin{bmatrix} L_{\mathrm{ac}} x_1 \\ C_{\mathrm{dc}} x_2 \end{bmatrix}. \tag{12}$$

The control of (12) has the same effect as controlling $[x_1, x_2]^{\mathrm{T}}$ except for a difference in the gains. It is clear from (10)–(12) that the targeted system is highly nonlinear and highly coupled. Moreover, $\boldsymbol{g}(\boldsymbol{x})$ has a piecewise form, which further complicates the controller design.

B. Design Procedures of the Proposed Nonlinear APD Control

By differentiating (12) once, one has

$$\dot{\boldsymbol{y}} = \begin{cases} \begin{bmatrix} v_{\mathrm{ac}} \\ -i_{\mathrm{load}} \end{bmatrix} + \begin{bmatrix} -x_2 & 0 \\ x_1 & -\frac{(x_2 - x_3)}{c} \end{bmatrix} \begin{bmatrix} u_1 \\ u_2 \end{bmatrix}, \text{ buck mode} \\ \begin{bmatrix} v_{\mathrm{ac}} \\ -i_{\mathrm{load}} \end{bmatrix} + \begin{bmatrix} -x_2 & 0 \\ x_1 & \frac{x_3^2}{(x_2 - x_3)c} \end{bmatrix} \begin{bmatrix} u_1 \\ u_2 \end{bmatrix}, \text{ boost mode.} \end{cases} \tag{13}$$

It is noted that the first derivative of $\boldsymbol{y}$ contains the control input $\boldsymbol{u}$. If the new control input $\boldsymbol{v}$ is selected as

$$\begin{bmatrix} \dot{y}_1 \\ \dot{y}_2 \end{bmatrix} = \begin{bmatrix} v_1 \\ v_2 \end{bmatrix} = \boldsymbol{v} \tag{14}$$

the original nonlinear and coupled system is then transformed into two decoupled and linear first-order SISO subsystems with respect to $\boldsymbol{v}$. The decoupling control law can be derived by solving (13) and (14) as

$$\boldsymbol{u} = \begin{cases} \begin{bmatrix} \frac{v_{\mathrm{ac}} - v_1}{x_2} \\ \frac{c[(v_{\mathrm{ac}} - v_1)x_1 - (v_2 + i_{\mathrm{load}})x_2]}{x_2(x_2 - x_3)} \end{bmatrix}, \text{ buck mode} \\ \begin{bmatrix} \frac{v_{\mathrm{ac}} - v_1}{x_2} \\ \frac{c[(v_{\mathrm{ac}} - v_1)x_1 - (v_2 + i_{\mathrm{load}})x_2]}{x_2 x_3^2}(x_2 - x_3) \end{bmatrix}, \text{ boost mode.} \end{cases} \tag{15}$$

If the output feedback law is set as

$$\begin{bmatrix} v_1 \\ v_2 \end{bmatrix} = \begin{bmatrix} \dot{y}_1^* + \alpha_1 (y_1^* - y_1) \\ \dot{y}_2^* + \alpha_2 (y_2^* - y_2) \end{bmatrix} \tag{16}$$

then the resultant closed-loop error dynamics of the system become

$$\begin{cases} \dot{e}_1 + \alpha_1 e_1 = 0 \\ \dot{e}_2 + \alpha_2 e_2 = 0 \end{cases} \tag{17}$$

where $e_i = x_i^* - x_i$, and $1/\alpha_i = \tau_i$ is the corresponding time constant. α_i, thereby, directly determines the bandwidth of the control loop of x_i and is a free design choice. The bandwidth of each control loop should be lower than the switching frequency but sufficiently high to achieve fast reference tracking. By properly designing the bandwidth, asymptotic reference tracking of the reference with a desirable rate of convergence can be achieved.

Finally, with reference to (15), the averaged i_{PPB} over T_{sw} can be derived as

$$i_{\mathrm{PPB}} = \frac{(v_{\mathrm{ac}} - v_1)\, x_1 - (v_2 + i_{\mathrm{load}})\, x_2}{x_2}. \tag{18}$$

Thus, the operating mode of the PPB can be conveniently determined by checking the polarity of $i_{\rm PPB}$ in (18), as mentioned in Section IV-A.

C. Stability Analysis of the Proposed Nonlinear APD Control

According to (17), e_1 and e_2 will always converge to zero if $\alpha_i > 0$. This means that y_1 and y_2 will track their respective references with zero steady-state errors and have global stability theoretically. However, the dynamics of the remaining state x_3, which is not directly controlled, can be described by the internal dynamic equation

$$\dot{x}_3 = a\left(x_3, \boldsymbol{y}, \boldsymbol{v}\right). \tag{19}$$

The stability of the internal dynamics, thus, solely determines the stability of the overall system. To simplify the analysis, it is sufficient to examine only the zero dynamics of x_3, i.e., when the system's tracking errors are zero, and thus,

$$\dot{x}_3 = a\left(x_3, \boldsymbol{y}^*, \dot{\boldsymbol{y}}^*\right). \tag{20}$$

1) Buck-Mode Operation: According to (10)–(16), the internal dynamics of x_3 during buck-mode operation are described by

$$\dot{x}_3 = \frac{1}{C_b x_3} \cdot \{x_1 \left[v_{\rm ac} - L_{\rm ac}\dot{x}_1^* - \alpha_1 L_{\rm ac}\left(x_1^* - x_1\right)\right] - x_2\left[i_{\rm load} + \alpha_2 C_{\rm dc}\left(x_2^* - x_2\right)\right]\}. \tag{21}$$

When the tracking errors of x_1 and x_2 tend to zero (i.e., $x_1 \rightarrow x_1^*, x_2 \rightarrow x_2^*$), the zero dynamics becomes

$$\dot{x}_3 = \frac{1}{C_b x_3} \cdot \left[x_1^*\left(v_{\rm ac} - L_{\rm ac}\dot{x}_1^*\right) - x_2^* i_{\rm load}\right]. \tag{22}$$

Without loss of generality, assume that

$$v_{\rm ac} = V_{\rm ac}\sin\left(\omega t\right), x_1^* = I_{\rm ac}^*\sin\left(\omega t + \theta^*\right). \tag{23}$$

Then, (22) is equivalent to

$$\frac{d}{dt}\left(x_3^2\right) = \frac{1}{C_b}\left[V_{\rm ac} I_{\rm ac}^* \cos\theta^* - 2x_2^* i_{\rm load} - V_{\rm in}^* I_{\rm ac}^* \sin\left(2\omega t + \theta^* + \varphi\right)\right] \tag{24}$$

where

$$V_{\rm in}^* = \sqrt{\left(V_{\rm ac} + \omega L_{\rm ac} I_{\rm ac}^* \sin\theta^*\right)^2 + \left(\omega L_{\rm ac} I_{\rm ac}^* \cos\theta^*\right)^2},$$
$$\varphi = \arctan\frac{V_{\rm ac} + \omega L_{\rm ac} I_{\rm ac}^* \sin\theta^*}{\omega L_{\rm ac} I_{\rm ac}^* \cos\theta^*}. \tag{25}$$

At the steady state, and according to the principle of conservation of energy, $I_{\rm ac}^*$ and θ^* should also satisfy

$$\frac{V_{\rm ac} I_{\rm ac}^*}{2}\cos\theta^* - x_2^* i_{\rm load} = 0. \tag{26}$$

Therefore, by solving the differential equation in (24) with the help of (26), x_3 can be resolved as

$$x_3 = \sqrt{V_{b0}^2 - A\cos\left(2\omega t + \theta^* + \varphi\right)} \tag{27}$$

where $A = \frac{V_{\rm in}^* I_{\rm ac}^*}{2\omega C_b}$, and V_{b0} is a constant that determines the offset value of x_3. Equation (27) indicates that x_3 is bounded by $\sqrt{{V_{b0}}^2 \pm A}$ and, thus, the zero dynamic is globally stable during the buck mode in the sense of Lyapunov.

2) Boost-Mode Operation: Following similar procedures, the zero dynamics of the system in boost-mode operation can be determined by

$$x_3 = \sqrt{V_{b0}^2 + A\cos\left(2\omega t + \theta^* + \varphi\right)}. \tag{28}$$

Equation (28) indicates that x_3 is bounded and, thus, the zero dynamics is globally stable in the sense of Lyapunov during boost mode.

D. Analysis on Robustness Against Parameter Variations

Feedback linearization typically requires the exact knowledge of the system parametric values. In practice, due to the component tolerances, temperature effect, etc., the actual component values will deviate from the nominal designed values. Deviation of the component values might affect the controller bandwidth and/or introduce state-state tracking errors. This can be explained by taking $C_{\rm dc}$ as an example. Assume that the actual output capacitance is $\tilde{C}_{\rm dc}$. Then, according to (12), the actual control output is

$$\tilde{y}_2 = \tilde{C}_{\rm dc} x_2. \tag{29}$$

Applying the same decoupling law (15), the second term in (14) then changes to

$$\dot{\tilde{y}}_2 = \dot{y}_2^* + \alpha_2\left(y_2^* - y_2\right). \tag{30}$$

Substitution of $\tilde{y}_2$ in (30) with (29) leads to

$$\tilde{C}_{\rm dc}\dot{x}_2 - C_{\rm dc}\dot{x}_2^* = \alpha_2 C_{\rm dc}\left(x_2^* - x_2\right). \tag{31}$$

As $\dot{x}_2^* \equiv 0$, (31) is identical to

$$\tilde{C}_{\rm dc}\left(\dot{x}_2^* - \dot{x}_2\right) + \alpha_2 C_{\rm dc}\left(x_2^* - x_2\right) = 0$$
$$\Leftrightarrow \dot{e}_2 + \alpha_2\frac{C_{\rm dc}}{\tilde{C}_{\rm dc}} e_2 = 0. \tag{32}$$

Equation (32) indicates that e_2 will still converge to zero, but with a time constant of $\tilde{\tau}_2 = \frac{1}{\alpha_2}\frac{\tilde{C}_{\rm dc}}{C_{\rm dc}}$. Compared to the error dynamics in (17), the deviation of the time constant from the designed value is proportional to the deviation of the capacitance. The dynamic waveforms of $v_{\rm dc}$ with different $C_{\rm dc}$ values are shown in Fig. 9(a). In this simulation, the reference x_2^* is step changed from 400 to 450 V. Also, the cases in which $C_{\rm dc}$ has a deviation of $\pm 20\%$ of the nominal value (10 μF) are tested in contrast to the case with no deviation of $C_{\rm dc}$. It can be observed that zero steady-state error is achieved in all the three scenarios but with a slight difference in the settling time.

By following a similar procedure, the impact of component variations in $L_{\rm ac}, L_b$, and C_b on the system's dynamic performance can be evaluated. It is concluded that: 1) variation of L_b only leads to a change in the control bandwidth, similar to the scenario of $C_{\rm dc}$ variation; 2) variation of $L_{\rm ac}$ leads to both steady-state tracking errors and a change in the control bandwidth. However, provided that the bandwidth of the line current tracking loop is sufficiently higher than the line frequency, the

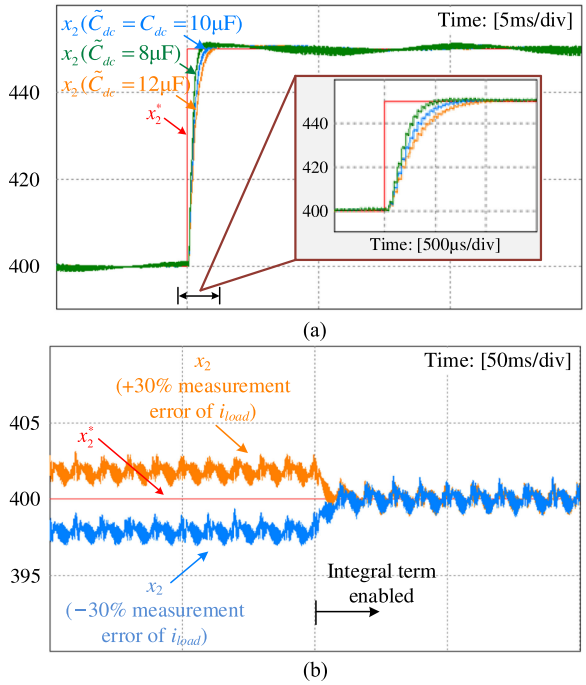

Fig. 9. (a) Response waveforms of the dc-port voltage under the reference step change with the dc-port capacitance tolerances of 0%, −20%, and +20%. (b) Waveforms of the dc-port voltage without and with the integral terms in the presence of a i_{load} measurement error of ±30%.

steady-state tracking error is negligible; and 3) variation of C_b does not affect the system's dynamic performance.

It is possible to further improve the system's performance by incorporating integral terms into the feedback law as in (33) to eliminate any residual steady-state errors due to the unmodeled dynamics, and/or sensing/control errors

$$\begin{bmatrix} v_1 \\ v_2 \end{bmatrix} = \begin{bmatrix} \dot{y}_1^* + \alpha_{11}\left(y_1^* - y_1\right) + \alpha_{12}\int\left(y_1^* - y_1\right)dt \\ \dot{y}_2^* + \alpha_{21}\left(y_2^* - y_2\right) + \alpha_{22}\int\left(y_2^* - y_2\right)dt \end{bmatrix}. \quad (33)$$

The capability of ensuring zero steady-state error is justified by the resultant new error dynamics of the closed-loop system as

$$\begin{cases} \ddot{e}_1 + \alpha_{11}\dot{e}_1 + \alpha_{12}e_1 = 0 \\ \ddot{e}_2 + \alpha_{21}\dot{e}_2 + \alpha_{22}e_2 = 0. \end{cases} \quad (34)$$

To demonstrate the viability of the new control law (33) for steady-state error elimination, the simulated waveforms of v_{dc} without and with the integral terms ($\alpha_{21} = 4000, \alpha_{22} = 40$) are compared in Fig. 9(b), assuming an i_{load} measurement error of ±30% and a v_{dc} reference of 400 V. Initially, no integral term is included and dc tracking errors of +2 and –2 V, respectively, are observed. In contrast, after the integral terms are incorporated, the steady-state errors are effectively eliminated. The complete system block diagrams with the proposed nonlinear controller are shown in Fig. 10(a). The equivalent control diagrams are shown in Fig. 10(b). The reference generation for x_1, which includes the design of the phase-locked-loop and the compensator G_{b0}(s), have been extensively studied in the literature and are well known [25]. This paper will not repeat the details.

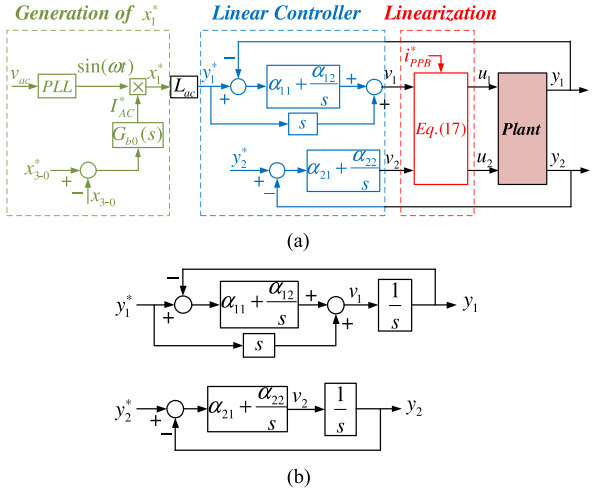

Fig. 10. (a) Control block diagram of the APD nonlinear controller for the targeted H^3 single-phase power converter. (b) Its equivalent control diagram after input–output feedback linearization.

E. Comparison With Linear Controllers

Fig. 11(a)–(c) illustrates the simulated waveforms of the converter using the 1) linear controller with DPD control strategy; 2) linear controller with APD control strategy; and 3) the proposed nonlinear controller with APD control strategy, respectively, for a step change of the dc voltage's reference from 400 to 450 V. With a load of 1.6 kΩ, the output power is switched from 100 to 127 W. The design of the linear controllers in Fig. 11(a) and (b) follows that in [9], with a control bandwidth identical to that of the proposed nonlinear controller.

According to Fig. 11, all three controllers achieve similar steady-state performances in terms of the power factor and output voltage regulation. However, Fig. 11(a) and (b) shows that the use of linear controllers, regardless of the control strategy, leads to a substantially delayed and disturbed step response of v_{dc} during the v_{dc} transient. The results confirm that the linear controller is less robust for large-signal operation of the converter. In contrast, with the proposed nonlinear control [see Fig. 11(c)], v_{dc} follows a first-order transfer function with a settling time of around 0.8 ms. This is expected with reference to the operating principle of the proposed control method as described in Section III.

V. Experimental Results

The proposed nonlinear APD controller is examined using both processor-in-the-loop PSIM simulations and a 100-W hardware prototype. The specifications of the simulated and experimentally tested system are shown in Table I. All control algorithms are implemented using a DSP (model no.: TMS320F28335) with a sampling frequency of 25 kHz. Unipolar sinusoidal-pulsewidth-modulation is employed to control the full-bridge converter. In the experiments, a programmable ac power supply (model no: PCR2000LE) is connected to the ac side of the converter directly and a resistor of 1.6 kΩ is used as the dc load. All the waveforms are captured using a digital oscilloscope (model no.: DSOX3024A).

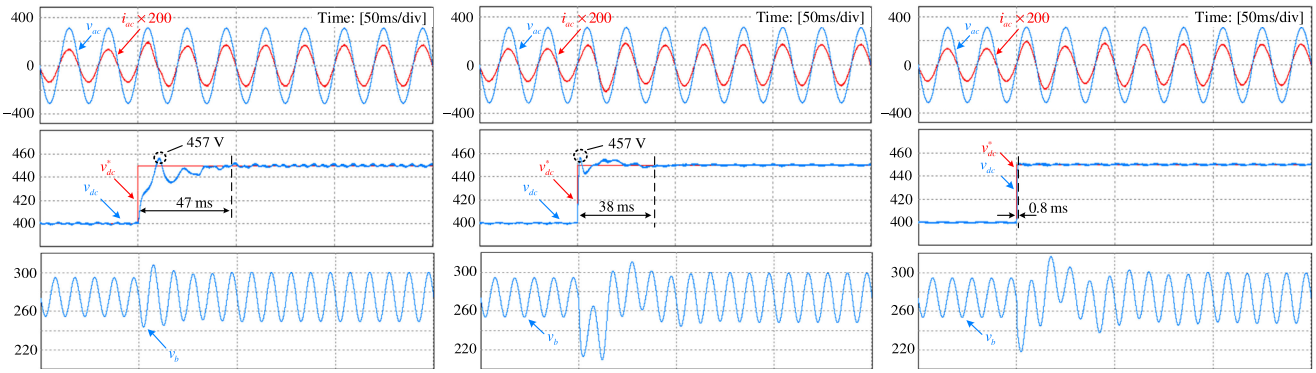

Fig. 11. Simulated waveforms of the converter for a step change of the dc voltage reference with (a) linear controller with DPD control strategy, (b) linear controller with APD control strategy, and (c) the proposed nonlinear control with APD control strategy.

TABLE I
SPECIFICATIONS OF TARGETED SINGLE-PHASE POWER CONVERTER WITH BUCK-TYPE PPB

Parameter		Value
rated power		100 W
switching frequency		25 kHz
switch model	S_1 to S_4	APT18M100B
	S_5, S_6	G4PC30FD
ac port	v_{ac}	220 V (RMS)/ 50 Hz
	L_{ac}	7 mH
dc port	V_{dc}	400 V
	C_{dc}	10 μF (film capacitor)
ripple port	C_b	30 μF (film capacitor)
	L_b	212 μH
	v_{b0}	275 V
controller	τ_1	250 μs
	τ_2	80 μs

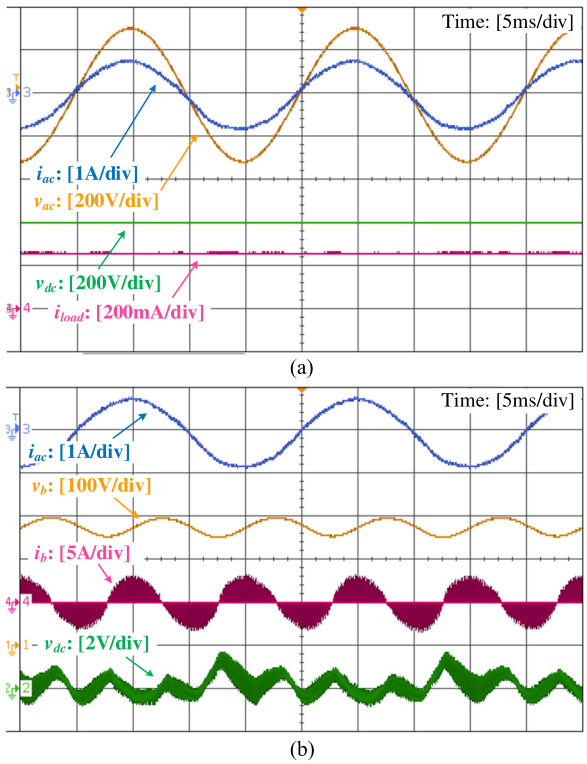

Fig. 12. Experimental steady-state waveforms of the single-phase power converter with the proposed nonlinear APD controller regarding (a) ac-port and dc-port performance and (b) ripple-port and control-output performance (The probe for measuring v_{dc} is ac coupled to provide an insight into the output-voltage regulation).

A. Steady-State Operation

Fig. 12 illustrates the steady-state operating waveforms of the power converter with the proposed nonlinear APD controller operating in rectifying mode of operation at full load. It can be observed that i_{ac} is in phase with v_{ac} with a low total harmonic distortion (THD) of 3.57%, and that the dc-link voltage v_{dc} is almost constant with a peak-to-peak voltage ripple Δv_{dc} of merely 2 V (0.5% of the average dc-link voltage). However, the voltage v_b across the energy storage ($C_b = 30\,\mu$F) is fluctuating significantly with a peak-to-peak voltage ripple of $\Delta v_b = 50$ V. The variation of v_b implies pulsating power buffering of the PPB. As a benchmark, C_b would be as large as 400 μF [1] with conventional passive buffering to achieve the same 0.5% dc-link ripple. In Fig. 12(b), the inductor L_b is operating in DCM as its current i_b reaches zero per switching cycle. A similar experiment is conducted at full load when the converter is operating as a grid-connected inverter. In this experiment, a dc-voltage source of 450 V (model no.: CPS-40003D in series with DP832) is connected to the dc-link of the converter through a $R_s = 100\,\Omega$ resistor [see Fig. 13(a)] to emulate a PV panel [2]. Again, the system achieves a unity power factor and a stable dc-link voltage, as shown in Fig. 14(a).

As the proposed controller is robust for large-signal operation, the energy storage can be further reduced and approach the theoretical limit (i.e., $C_b = 3.98\,\mu$F as predicted by [1]). Fig. 14(b) illustrates the operating waveforms of the converter as C_b is reduced to 5.47 μF in the rectifying mode of operation. While v_b has a large voltage swing of more than 300 V (75% of v_{dc}), the converter retains its unity power factor and the stable dc-link voltage. In practical applications, sufficient voltage

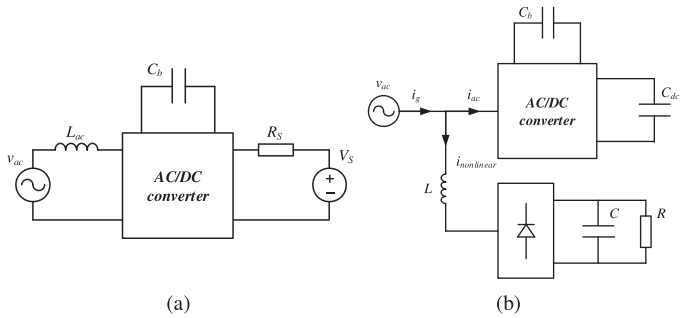

Fig. 13. (a) Circuit diagram of the inverter experiment. (b) Circuit diagram of the APF function experiment.

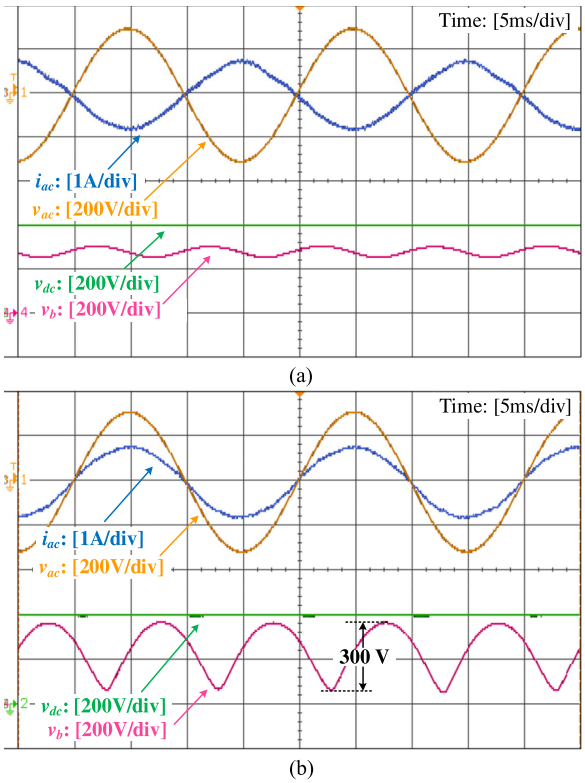

Fig. 14. Additional steady-state test of the converter. (a) Inverting operation with full load. (b) Operation with a reduced buffering capacitor (5.47 μF).

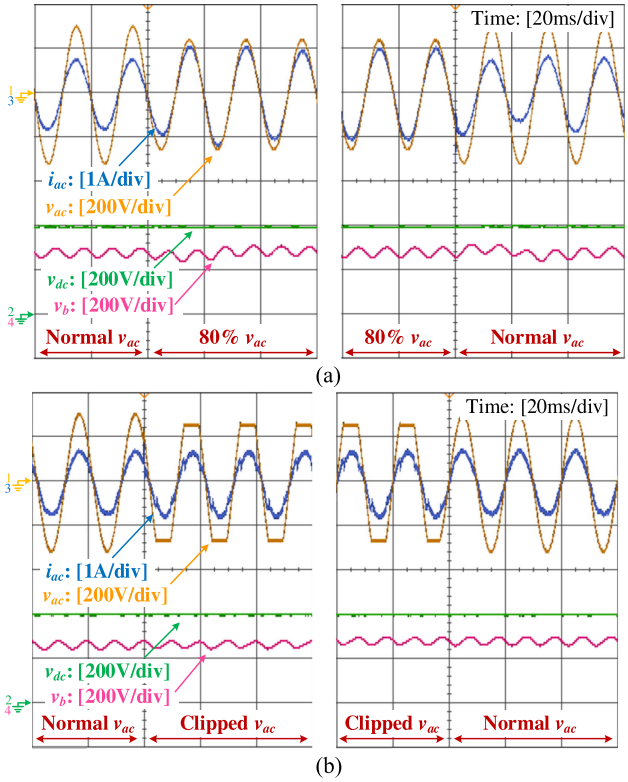

Fig. 15. Experimental transient waveforms of the converter regarding (a) input voltage sag of 20% and (b) input voltage clipping (crest factor of 1.2).

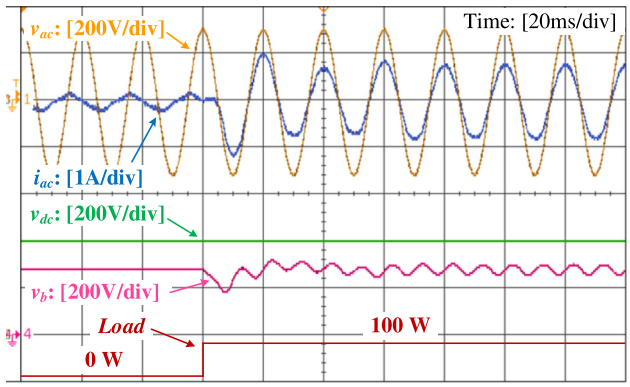

Fig. 16. Experimental transient waveforms of the converter regarding load step change from 0 to 100 W.

margin must be taken into consideration such that v_b always stays between 0 V and v_{dc} reliably even in the event of transient intervals. Therefore, $C_b = 30\,\mu$F is reused in the following transient tests. The objective of the experiment in Fig. 14(b), however, is to demonstrate the capabilities of the controller for large-signal operation and to confirm that the ac-port and the dc-port are fully decoupled from the ripple-port dynamics.

B. Transient Performance

1) Input-Voltage-Disturbance Rejection: The dynamic responses of the converter with the proposed control to 1) a step change of v_{ac} ($\pm$20%); and 2) ac voltage clipping (crest factor = 1.2), are recorded in Fig. 15. In both scenarios, v_{dc} is shown to be almost immune to the imposed input voltage disturbances and remains tightly regulated before, during, and after the transient intervals. The dynamics of the dc-port can, thus, be regarded as decoupled from that of the ac-port. However, unity power factor is still retained at the ac side throughout the transient interval. The measured THDs are 2.62% and 7.73%, respectively, during voltage sag and voltage clipping tests. The slightly increased THD during the voltage clipping test is due to the small current spikes in i_{ac}, as shown in Fig. 15(b) (occurred at the voltage-clipping instant and are caused by the front-end EMI filter, which is interfacing with the distorted ac voltage).

2) Load-Disturbance Rejection: Fig. 16 demonstrates the dynamic responses of the converter as the dc load is switching from no load to full load. The dc-link voltage is again shown to be very robust and can be regarded as decoupled from the load variations. A step change of the load power causes a step

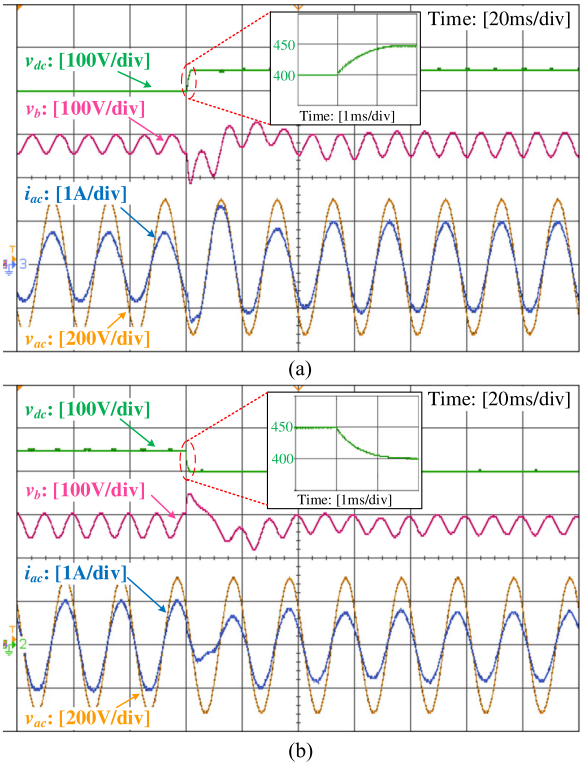

Fig. 17. Experimental transient waveforms of the converter regarding step change of output voltage reference (a) from 400 to 450 V and (b) from 450 to 400 V.

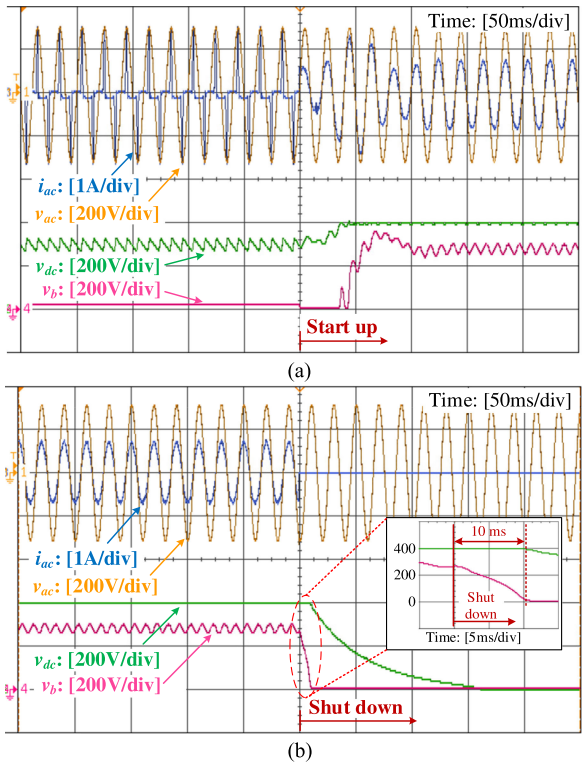

Fig. 18. Experimental waveforms of (a) startup (without soft start) and (b) shutdown processes.

change of power imbalance between the ac side and the dc side of the converter. With the APD control strategy, a step change of the imbalanced power can still be buffered automatically by C_b. The buffering of this "stepped" imbalanced power can be visualized in Fig. 16 as there is sudden voltage overshoot/undershoot in v_b at the load change instant.

3) Control Reference Tracking: The reference-tracking performance of the converter is also examined, and the results are recorded in Fig. 17. In this experiment, the dc voltage reference V_{dc}^* is step changed between 400 and 450 V with a resistive load of 1.6 kΩ at the dc side. As highlighted in the zoomed-in part of Fig. 17, v_{dc} has a typical first-order response with a settling time of around 1.5 ms for both voltage step-up and step-down tests. These observations confirm the theoretical analysis in Section IV that the closed-loop error dynamics are of first order, and match closely the designed dc-loop time constant of 0.25 ms. A step change of v_{dc} causes a stepped power imbalance due to 1) a step change of load power between 100 and 127 W; and 2) a sudden charging/discharging power of $C_{dc}v_{dc}(dv_{dc}/dt)$ for C_{dc}. The "stepped" power imbalance is again buffered automatically by C_b, leading to sudden voltage variations in v_b.

C. Direct Startup and Active Voltage Holdup

System startup and shutdown essentially involve large-signal operation. To start up reliably, the reference commands for startup control are usually incremented in a staircase manner slowly toward the final set values. This process is known as soft start. With the aid of the proposed nonlinear APD controller, which is robust in large-signal operation, the power converter can be directly started up quickly toward full power without the soft-start process. The startup waveforms with the proposed control are captured and shown in Fig. 18(a). Prior to startup, v_{dc} has been charged up to around 300 V by the ac source through the body diodes of the full-bridge switches (i.e., S_1 to S_4). The converter is then started up directly by switching to the proposed nonlinear APD controller. As Fig. 18(a) illustrates, v_{dc} reaches the set reference V_{dc}^* quickly within 50 ms. Unlike the reference-tracking test in the previous section, v_{dc} does not follow the expected first-order responses, and the settling time is much longer than the expected 1.5 ms. The reason is that C_b does not have enough energy to charge up v_{dc} at the beginning of the startup (i.e., $v_b = 0$ V). Instead, v_{dc} is gradually charged up by the ac voltage source. After v_b is elevated with sufficient energy, v_{dc} then quickly settles to the targeted reference V_{dc}^*.

However, the shutdown waveforms of the converter are recorded in Fig. 18(b). As mentioned in the introduction, holdup function is mandatory in many applications. Typical holdup time is half to one line cycle, i.e., 10 to 20 ms for a 50 Hz grid [26]. Due to the small energy-storage capacitor used in the H^3 single-phase power converter, there has been a misconception that these converters may not be suitable for providing holdup function. Fig. 18(b) has demonstrated, for the first time, that v_{dc} is actually held constant at 400 V for as long as 10 ms after the ac voltage is shut down, and that H^3 single-phase power converters *can* meet the holdup requirement just as the conventional single-phase converters. The continued regulation of v_{dc} is feasible as the large-signal model in (10) still governs the system's dynamics

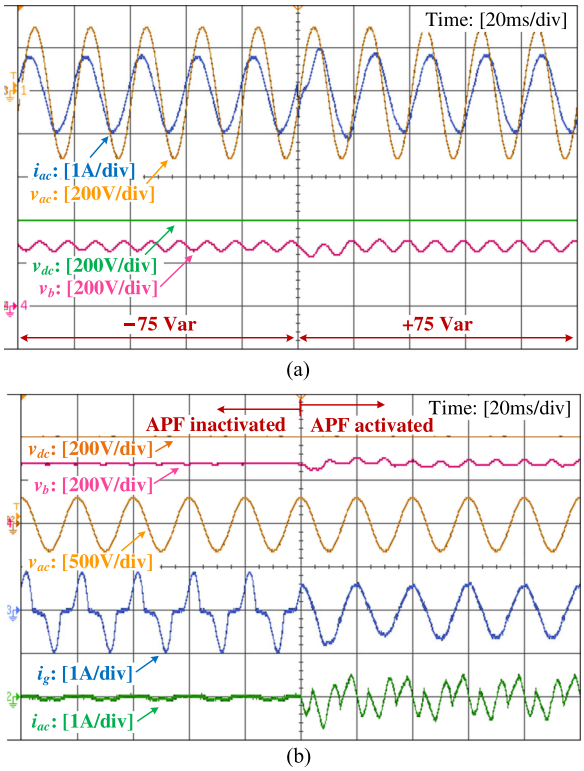

Fig. 19. Ancillary service tests of the proposed nonlinear APD control with respect to (a) reactive power generation and (b) APF.

after the converter is disconnected from $v_{\rm ac}$. Thus, the nonlinear APD control is still effective for system regulation. As a result, the energy stored in C_b can be fully utilized to actively sustain the output power. Once C_b is fully discharged (i.e., when $v_b = 0\,\text{V}$), $v_{\rm dc}$ begins to decrease as enough energy is not available to support the dc-link voltage. Compared to the passive holdup solutions in conventional single-phase converters (i.e., using large dc-link capacitors), the active holdup function can fully exploit the potential of the energy storage, and significantly reduce the energy-storage requirement.

D. Provision of Ancillary Services

In many practical applications, the voltage source converters are expected to provide some ancillary services, such as reactive power generation and APF, while still supplying/generating the real power desired. Some preliminary results are obtained to demonstrate the feasibilities of having a *multifunctional* H^3 single-phase power converter for the first time, as illustrated in Fig. 19.

Fig. 19(a) demonstrates the captured waveforms of the converter when it is supplying a reactive power of -75 and $+75$ var to the grid while at the same time outputting 100 W of real power to the dc load. The step change of the reactive power is achieved by changing the power angle (the phase difference between $i^*_{\rm ac}$ and $v_{\rm ac}$) in the ac current control loop. As observed in Fig. 19(a), the phase angle of $i_{\rm ac}$ is changed abruptly while still maintaining a stable dc-link voltage (or the dc power).

To demonstrate the feasibility of performing the APF function with the H^3 single-phase converter, a single-phase diode-bridge rectifier with an RC load ($R = 800\,\Omega, C = 20\,\mu\text{F}$) is connected through an inductor ($L = 150\,\text{mH}$) to the same ac-voltage source to which the H^3 single-phase converter is connected [as configured in Fig. 13(b)]. The diode-bridge load draws a nonlinear current $i_{\rm nonlinear}$ and is used as the harmonics source in the experiment. To maintain a sinusoidal line current i_g flowing into the ac voltage source, $i_{\rm nonlinear}$ must be actively compensated. This is achieved by sensing $i_{\rm nonlinear}$, extracting its harmonic components, and then imposing them on the original $i^*_{\rm ac}$ reference command, as shown in Fig. 10(a). The measured waveforms before and after the activation of APF function are demonstrated in Fig. 19(b). It is shown that the THD of i_g is drastically reduced from 52.9% down to 6.03% as the APF function is activated. In the meantime, $v_{\rm dc}$ is still well regulated at 400 V after APF is enabled. The instantaneous power absorbed by the H^3 power converter, which is highly nonlinear, can be clearly visualized from the distorted waveforms of v_b.

VI. Conclusion

In this paper, we proposed a general nonlinear controller for improving the performance the emerging class of high power density, high power-conversion efficiency, and high reliability (H^3) single-phase power converters featuring small buffering capacitance. Based on generic network modeling, it is shown that H^3 single-phase power converters are inherently large-signal, highly nonlinear, and highly coupled MIMO systems. These new features justify the nonlinear approach adopted in this paper, which is based on input–output feedback linearization technique. A novel APD control strategy is also proposed to further enhance the dynamic performance and robustness against external disturbances. The proposed nonlinear APD controller is further extended to DCM system to demonstrate its feasibility. The presented control theory has been extensively examined both in simulations and experiments. Satisfactory transient performance and robustness are demonstrated. New opportunities for the development of H^3 single-phase power converters have been suggested with the aid of the proposed nonlinear APD control.

References

[1] P. T. Krein, R. S. Balog, and M. Mirjafari, "Minimum energy and capacitance requirements for single-phase inverters and rectifiers using a ripple port," *IEEE Trans. Power Electron.*, vol. 27, no. 11, pp. 4690–4698, Nov. 2012.

[2] GOOGLE, "Detailed inverter specifications, testing procedure, and technical approach and testing application requirements for the Little Box Challenge," Mountain View, Tech. Rep., 2015. [Online]. Available: https://www.littleboxchallenge.com/

[3] D. Bortis, D. Neumayr, and J. W. Kolar, "$\eta\rho$;-Pareto optimization and comparative evaluation of inverter concepts considered for the GOOGLE Little Box Challenge," in *Proc. IEEE 17th Workshop Control Model. Power Electron.*, Trondheim, Norway, 2016, pp. 1–5.

[4] Y. Lei *et al.*, "A 2-kW single-phase seven-level flying capacitor multilevel inverter with an active energy buffer," *IEEE Trans. Power Electron.*, vol. 32, no. 11, pp. 8570–8581, Nov. 2017.

[5] A. S. Morsy and P. N. Enjeti, "Comparison of active power decoupling methods for high-power-density single-phase inverters using wide-

bandgap FETs for google little box challenge," *IEEE J. Emerg. Sel. Top. Power Electron.*, vol. 4, no. 3, pp. 790–798, Sep. 2016.
[6] J. W. Kolar, D. Bortis, and D. Neumayr, "The ideal switch is not enough," in *Proc. 28th Int. Symp. Power Semicond. Devices ICs*, 2016, pp. 15–22.
[7] S. Li, G. Zhu, S. Tan, and S. Y. R. Hui, "Direct AC/DC rectifier with mitigated low-frequency ripple through inductor-current waveform control," *IEEE Trans. Power Electron.*, vol. 30, no. 8, pp. 4336–4348, Aug. 2015.
[8] Y. Tang, Z. Qin, F. Blaabjerg, and P. C. Loh, "A dual voltage control strategy for single-phase PWM converters with power decoupling function," *IEEE Trans. Power Electron.*, vol. 30, no. 12, pp. 7060–7071, Dec. 2015.
[9] S. Li, W. Qi, S.-C. Tan, and S. Y. R. Hui, "Enhanced automatic-power-decoupling control method for single-phase ac-to-dc converters," *IEEE Trans. Power Electron.*, vol. 33, no. 2, pp. 1816–1828, Feb. 2018.
[10] D. Neumayr, D. Bortis, and J. W. Kolar, "Ultra-compact power pulsation buffer for single-phase dc/ac converter systems," in *Proc. IEEE 8th Int. Power Electron. Motion Control Conf.*, 2016, pp. 2732–2741.
[11] A. Anup, Y. Yang, and F. Blaabjerg, "Thermal performance and reliability analysis of single-phase PV inverters with reactive power injection outside feed-in operating hours," *IEEE J. Emerg. Sel. Top. Power Electron.*, vol. 3, no. 4, pp. 870–880, Dec. 2015.
[12] B. Wang, X. Ruan, K. Yao, and M. Xu, "A method of reducing the peak-to-average ratio of LED current for electrolytic capacitor-less AC–DC drivers," *IEEE Trans. Power Electron.*, vol. 25, no. 3, pp. 592–601, Mar. 2010.
[13] R. Wang *et al.*, "A high power density single-phase PWM rectifier with active ripple energy storage," *IEEE Trans. Power Electron.*, vol. 26, no. 5, pp. 1430–1443, May 2011.
[14] L. Han and N. Narendran, "An accelerated test method for predicting the useful life of an LED driver," *IEEE Trans. Power Electron.*, vol. 26, no. 8, pp. 2249–2257, Aug. 2011.
[15] S. Wang, X. Ruan, K. Yao, S. C. Tan, Y. Yang, and Z. Ye, "A flicker-free electrolytic capacitor-less AC–DC LED driver," *IEEE Trans. Power Electron.*, vol. 27, no. 11, pp. 4540–4548, Nov. 2012.
[16] S. B. Kjaer, J. K. Pedersen, and F. Blaabjerg, "A review of single-phase grid-connected inverters for photovoltaic modules," *IEEE Trans. Ind. Appl.*, vol. 41, no. 5, pp. 1292–1306, Sep. 2005.
[17] S. Li, W. Qi, S.-C. Tan, and S. Y. R. Hui, "A single-stage two-switch PFC rectifier with wide output voltage range and automatic AC ripple power decoupling," *IEEE Trans. Power Electron.*, vol. 32, no. 9, pp. 6971–6982, Sep. 2017.
[18] H. Li, K. Zhang, H. Zhao, S. Fan, and J. Xiong, "Active power decoupling for high-power single-phase PWM rectifiers," *IEEE Trans. Power Electron.*, vol. 28, no. 5, pp. 1308–1319, Mar. 2013.
[19] S. Li, W. Qi, S. Tan, and S. Y. R. Hui, "Integration of an active filter and a single-phase AC/DC converter with reduced capacitance requirement and component count," *IEEE Trans. Power Electron.*, vol. 31, no. 6, pp. 4121–4137, Jun. 2016.
[20] Q.-C. Zhong, and W.-L. Ming, "A θ;-converter that reduces common mode currents, output voltage ripples, and total capacitance required," *IEEE Trans. Power Electron.*, vol. 31, no. 12, pp. 8435–8447, Dec. 2016.
[21] Y. Liu, Y. Sun, M. Su, X. Li, and S. Ning, "A single phase AC/DC/AC converter with unified ripple power decoupling," *IEEE Trans. Power Electron.*, vol. 33, no. 4, pp. 3204–3217, Apr. 2018.
[22] J.-J. E. Slotine and W. Li, "Feedback linearization" in *Appl. Nonlinear Control*, 6th ed., vol. 199, no. 1. Upper Saddle River, NJ, USA: Prentice-Hall, 1991, pp. 207–271.
[23] D. I. Kim, I. J. Ha, and M. S. Ko, "Control of induction motor via feedback linearization with input–output decoupling," *Int. J. Control*, vol. 51, no. 4, pp. 863–886, Mar. 1990.
[24] D.-C. Lee, G.-M. Lee, and K.-D. Lee, "DC-bus voltage control of three-phase AC/DC PWM converters using feedback linearization," *IEEE Trans. Ind. Appl.*, vol. 36, no. 3, pp. 826–833, May/Jun. 2000.
[25] M. Ciobotaru, R. Teodorescu, and F. Blaabjerg, "A new single-phase PLL structure based on second order generalized integrator," in *Proc. 37th IEEE Power Electron. Spec. Conf.*, Jeju, South Korea, 2006, pp. 1–6.
[26] Y. Jang, M. M. Jovanovic, and D. L. Dillman, "Hold-up time extension circuit with integrated magnetics," *IEEE Trans. Power Electron.*, vol. 21, no. 2, pp. 394–400, Mar. 2006.

Huawei Yuan (S'16) received the B.E. and M.E. degrees in electrical engineering from Tsinghua University, Beijing, China, in 2013 and 2016, respectively. He is currently working toward the Ph.D. degree at the Department of Electrical and Electronic Engineering, the University of Hong Kong, Hong Kong.

His current research interests include nonlinear control of power converters and renewable energy.

Sinan Li (M'14) received the B.S. degree in electrical engineering from the Harbin Institute of Technology, Harbin, China, in 2009, and the Ph.D. degree in electrical and electronic engineering from The University of Hong Kong, Hong Kong, China, in 2014.

He is currently a Postdoctoral Research Fellow with the Department of Electrical and Electronic Engineering, The University of Hong Kong. He has authored or coauthored more than 40 transaction papers and conference papers. He also holds five U.S. patents, and three of these patents have been adopted by industry. His current research interests include power electronics and control, wireless power transfer, renewable energy, and smart grids.

Dr. Li is a Founding Member of IEEE-Eta Kappa Nu (HKN) at The University of Hong Kong.

Wenlong Qi (S'14) received the B.E. and M.E. degrees from the Shandong University, Jinan, China, in 2011 and 2014, respectively. He is currently working toward the Ph.D. degree in the Department of Electrical and Electronic Engineering, The University of Hong Kong, Hong Kong.

He has authored or coauthored more than 10 transaction papers and conference papers. He also holds two Chinese patents. His current research areas include nonlinear control technique and single-phase inverters and rectifiers.

Siew-Chong Tan (S'00–M'06–SM'11) received the B.Eng. (Hons.) and M.Eng. degrees in electrical and computer engineering from the National University of Singapore, Singapore, in 2000 and 2002, respectively, and the Ph.D. degree in electronic and information engineering from the Hong Kong Polytechnic University, Hong Kong, in 2005.

From October 2005 to May 2012, he worked as a Research Associate, Postdoctoral Fellow, Lecturer, and Assistant Professor with the Department of Electronic and Information Engineering, Hong Kong Polytechnic University, Hong Kong. From January to October 2011, he was a Senior Scientist with the Agency for Science, Technology and Research (A∗Star), Singapore. He is currently an Associate Professor with the Department of Electrical and Electronic Engineering, The University of Hong Kong, Hong Kong.

Dr. Tan serves extensively as a reviewer for various IEEE/IET transactions and journals on power, electronics, circuits, and control engineering. He is a co-author of the book *Sliding Mode Control of Switching Power Converters: Techniques and Implementation* (CRC Press, 2011).

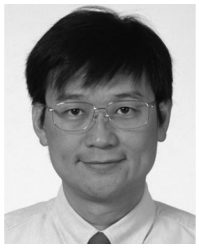

Shu-Yuen (Ron) Hui (M'87–SM'94–F'03) received the B.Sc.(Hons.) Eng. degree in electrical and electronic engineering from the University of Birmingham, Birmingham, U.K., in 1984, and the D.I.C. and Ph.D. degrees from Imperial College London, London, U.K., in 1987.

Since July 2010, he has been concurrently a part-time Chair Professor of power electronics with Imperial College London and Philip Wong Wilson Wong Professor with The University of Hong Kong, Pokfulam, Hong Kong. He has authored or coauthored more than 260 refereed journal publications and book chapters, and more than 60 of his patents have been adopted by industry. Dr. Hui is an Associate Editor for the IEEE TRANSACTIONS ON POWER ELECTRONICS and the IEEE TRANSACTIONS ON INDUSTRIAL ELECTRONICS. He is the recipient of the 2010 IEEE Rodulf Chope R&D Award from the IEEE Industrial Electronics Society, 2010 IET Crompton Medal, and 2015 IEEE William E. Newell Power Electronics Award.

Dr. Hui is a Fellow of the Australian Academy of Technological Sciences and Engineering and also the Royal Academy of Engineering (U.K.).